



Porous carbon nanofibers derived from PAA-PVP electrospun fibers for supercapacitor

Tie-Shi He^{1,2} · Xiao-Dong Yu¹ · Tian-Jiao Bai¹ · Xiang-Ye Li¹ · Yi-Ran Fu¹ · Ke-Di Cai^{1,2}

Received: 6 November 2019 / Revised: 13 February 2020 / Accepted: 9 March 2020 / Published online: 25 April 2020
© Springer-Verlag GmbH Germany, part of Springer Nature 2020

Abstract

The polyamic acid (PAA) and polyvinylpyrrolidone (PVP) blends electrospun fibers were prepared by electrospinning method. PAA with high carbon conversion served as carbon nanofibers; PVP with low carbon conversion served as porogenic sacrificial agent. Then, the PAA-PVP-based carbon nanofibers with well-controlled meso/macro pore structure were obtained via thermally induced phase separation process. The morphology and electrochemical performance of porous carbon nanofibers are investigated by structural analysis and electrochemical measurements. The relationship among pore structure, character of electrolyte and electrochemical performance of porous carbon nanofibers was extensively evaluated. Porous carbon nanofibers derived from PAA-PVP (mass ratio = 5:2) electrospun fibers show adjustable average pore diameter (3.1 nm), high BET specific surface area ($743.5 \text{ m}^2 \text{ g}^{-1}$), and average pore volume ($0.126 \text{ cm}^3 \text{ g}^{-1}$). The supercapacitor constructed by porous nanofibers as electrode in ionic liquids electrolyte exhibits wide electrochemical stability window (3.4 V), high specific capacity (211.7 F g^{-1}), good power density (2021 W kg^{-1}), and low internal resistance (1.0Ω). The findings reveal a guideline of the preparation of blending polymer-based porous carbon nanofibers for electrochemical energy conversion and storage.

Keywords Porous carbon nanofibers · Thermally induced phase separation · Electrospun · Polyamic acid · Ionic liquids · Supercapacitor

Introduction

Supercapacitor is one of most promising electrochemical energy storage devices owing to its high power density, rapid charging/discharging ability, and long cycle life [1]. However, the low working potential and energy density of conventional supercapacitor limit its widespread applications [2], such as renewable energy generation [3] and electric vehicles and 5G mobile communication [4]. Energy density (E) and power density (P) of supercapacitor are in direct ratio to the square of working potential (V) ($2E = CV^2$, $4P = V^2 (R \cdot m)^{-1}$, C is the specific capacity, V is the working potential, R is the internal resistance, m is the mass of electrode materials) [5], so how to

improve working potential of supercapacitor is a key factor for the preparation of supercapacitor with high capacitance and rate capability [6]. The working potential of supercapacitor is to depend on seriously the character of electrolyte. The working potential of aqueous electrolyte and organic electrolyte is below 1.0 V [7] and 3.0 V [8], respectively, which is due to the low decomposition voltage of the water and organic solvent in electrolyte.

Recently, the successful utilization of room temperature ionic liquids (ILs) as electrolyte in supercapacitor has demonstrated its high electrochemical performance. The solvent-free and wide electrochemical stability window ($\geq 5.0 \text{ V}$) of ILs can provide high working potential [9]. Furthermore, high concentration ($\geq 3.0 \text{ mol L}^{-1}$) of ILs can also contribute higher energy density to supercapacitor ($E \propto C_{\text{electrolyte concentration}}$) [10]. However, ILs has larger molecular/ion size and higher viscosity than the electrolyte based on aqueous or organic solvent [11], thus, the adjustment between pore structure of electrode materials and ILs, which is necessary for high utilization of pores, fast ion mobility/diffusibility, and short electrical double layers (EDLs) forming time. So the preparation of new porous electrode materials and the investigation of interaction

✉ Tie-Shi He
hetieshi@163.com

¹ School of Chemistry & Chemical Engineering, Bohai University, Jinzhou 121013, China

² Liaoning Engineering Technology Center of Supercapacitor, Jinzhou 121000, China

between electrode materials and ILs are critical for the improvement of power and energy density of supercapacitor.

Nano-structure porous materials as electrode have highly specific surface area, fast charge transport ability and highly exposed electrode-electrolyte interface, so they play a crucial role for the development of high electrochemical performance supercapacitors [12], so they play a crucial role for the development of high electrochemical performance supercapacitor. Numerous synthetic procedures have been adopted for the synthesis of nanoparticles, nanosheets, and nanofibers for electrode materials of supercapacitor [13]. Carbon nanofibers with high aspect ratio, good conductivity, and simple processing become attractive electrode materials for supercapacitor. Among them, carbon nanofibers derived from electrospun polymer fibers are emerging electrode materials due to their simple procedure and scalability, in which ultralong one-dimensional carbon nanofibers can be easily prepared with various free-standing morphological features [14]. Carbon nanofibers can be prepared via interfacial polymerization [15], vapor deposition [16], electrospinning process, and so on. Carbon nanofibers derived from electrospun fibers, such as polyacrylonitrile [17], phenolic resins [18], and polyamic acid (PAA) [19], have been widely studied and applied. Among them, PAA is used as the precursor for carbon nanofibers of electrode materials [20] due to its high carbon yield, good graphite-like crystallite, and flexible free-standing fiber mats structure etc. [21].

Carbon nanofibers derived from electrospun PAA fibers have been subjected to physical or chemical process [22] to increase their specific surface area and porosity; however, the average pore radius of conventional carbon nanofibers is less than 1 nm in dimensions [23], causing low utilization of porosity and mobility/diffusibility of ions as electrode materials of supercapacitor in ILs. Thus, supercapacitor constructed by carbon nanofibers with well-designed hierarchical pores as electrode materials will exhibit better electrochemical performance in ILs.

Preparation of porous [24] carbon nanofibers derived from electrospun PAA blends sacrificial polymer via phase-separated method is simple and practicable process; however, the control over the pore size, volume, and uniformity remains challenging [25]. In this regard, the PAA and polyvinylpyrrolidone (PVP) blends electrospun nanofibers are prepared. Then, the PAA with high carbon conversion is transformed into carbon framework, and the PVP with low carbon conversion is served as porogen to generate pores via thermally induced phase separation, so the porous carbon nanofibers were obtained from PAA-PVP electrospun fibers. The pore structure parameters of PAA-PVP-based carbon nanofibers derived from various mass ratios of PAA and PVP are studied, and the correlations among the electrochemical feature, pore

structures [26] of carbon nanofibers, and ILs electrolyte are systematically elucidated. Additionally, this work also provides a well-controlled method for the preparation and application of porous nanofibers [27] in energy storage, separation, and catalysis etc.

Experimental

Material and instrument

All materials and reagents were purchased from Tianjin Chemical Reagent Co. and were used without further purification unless otherwise specified. The specific surface area and pore size distribution of nanofibers were tested by the nitrogen adsorption at 77 K (SSA-4200, Builder Corporation, China) and calculated using the Brunauer-Emmett-Teller (BET) and the Barrett-Joyner-Halenda (BJH) methods, respectively [28]. Thickness of electrospun nanofiber mats was determined by thickness tester (CHY-C2). The morphology feature of the nanofibers was observed by scanning electron microscopy (SEM; Hitachi S-4800). The thermal stability of the polymer was measured by thermal gravimetric (TG) analysis with 10 °C min⁻¹ scanning rate from room temperature to 800 °C under nitrogen ambience (Diamond TG/DTA, USA).

Preparation of porous carbon nanofibers

Preparation of PAA-PVP electrospun fibers PAA was synthesized with 0.5 mol pyromellitic acid dianhydride ($M_w = 218.12 \text{ g mol}^{-1}$) and 0.5 mol 4,4'-oxydianiline ($M_w = 200.24 \text{ g mol}^{-1}$) in 50 mL *N,N'*-dimethylformamide (DMF) [29]. Above solution was stirred under Ar ambience at 0 °C for 12 h. The 15 wt% precursor solution was prepared by mixing the PAA and PVP ($M_w = 380,000 \text{ g mol}^{-1}$) in DMF; the mass ratio of PAA:PVP is 5:1, 5:2, and 5:5, respectively. The subsequent electrospinning was performed under ambient condition, 18-kV positive voltage, 13-cm working distance (the distance between the needle tip and the target), and 1.0 mL h⁻¹ flow rate [30]. A copper net served as the collector and the collection time was set at 3.0 h. The prepared electrospun fiber mats were vacuum dried at 40 °C for 12 h to remove any traces of solvent residue.

Preparation of porous carbon nanofibers Pyrolysis of carbon nanofibers was performed in a tubular furnace (OTF-1200X, MIT Corporation) under the following conditions: room temperature to 280 °C within 2 h in air ambience, and then changed to 20 cm³ min⁻¹ Ar flow, from 280 to 900 °C within 7 h. The carbonized PAA-PVP electrospun fibers were activated by KOH at 850 °C for 2.0 h directly after carbonization [31].

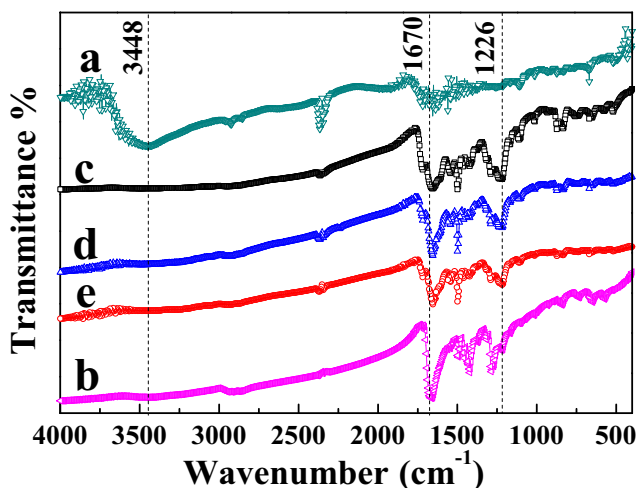


Fig. 1 FTIR of polymer electrospun fibers. Mass ratio of PAA:PVP (a) 5:0, (b) 0:5, (c) 5:1, (d) 5:2, (e) 5:5

Preparation of porous carbon nanofiber electrode supercapacitor

Porous carbon fibers were chosen as the negative and positive electrode materials for the supercapacitors. Carbon nanofibers mats with around 200 μm in thickness were cut into 2.0 cm² pieces and pasted on the surface of stainless steel capacitor case using conductive adhesive (TEN20 EEG). The carbon fiber capacitor case and separator (25 μm polypropylene membrane, Celgard) were subsequently vacuum dried at 120 °C for 24 h. The separator (25 μm polypropylene membrane, Celgard) was soaked in ILs (*N,N'*-diethyl-*N*-methyl-*N*-(2-methoxyethyl) ammonium tetrafluoroborate ([DEMETFSA]BF₄⁻, Lanzhou Greenchem ILs). All the experimental materials were dried at 120 °C for 24 h before being assembled in an Ar-filled glove box (H₂O and O₂ < 10 mg L⁻¹).

Characterization of supercapacitor

Electrochemical measurements were performed in a two-electrode disc-type capacitor [32]. The specific capacity measured was expressed as the charge stored per total mass of electrodes (F g⁻¹). The direct current internal resistance (*R*, Ω) was calculated from $R = \Delta U / I$, where Δ*U* (V) is potential

drop (*IR* drop) that was recorded at the beginning of the discharge process and *I* (A) is the discharge current. The specific capacity (*C*, F g⁻¹) of the electrode material was defined as $C = I \Delta V / m \Delta t$, where Δ*V* is the potential difference value, Δ*t* is the corresponding discharge time difference value, and *m* is the activated material content of both electrodes [33]. The energy density *E* (J g⁻¹ or Wh kg⁻¹) was calculated using $E = 0.5 C [(V_{\text{initial}} - \Delta U)^2 - V_{\text{final}}^2]$, where *V*_{initial}, *V*_{final}, and *I* stand for the initial potential, final potential, and discharging current, respectively. The power density (*P*, W kg⁻¹) was calculated according to the formula $P = E / t$. Charging/ discharging efficiency (*η*, %) is defined by $Q_{\text{discharge}} / Q_{\text{charge}}$.

Results and discussion

Morphology and structure of nanofibers

The inter-molecular interaction between PAA and PVP of PAA-PVP electrospun fibers was chartered by FTIR, as shown in Fig. 1. The characteristic peak of 1670 cm⁻¹ associated with stretching vibration of C=O of PAA-PVP, which has slightly red-shift (Figs. 1c, 1d, 1e) due to the influence of hyper-conjugation effect between benzene ring and pyridine ring structure of PAA-PVP (Fig. 2). The characteristic peak of 1670 cm⁻¹ related to stretching vibration of C=O of PAA-PVP, which has slightly red-shift (Fig. 1c, d, e) compared with PVP (Fig. 1b), can be attributed to the influence of hyper-conjugation effect between benzene ring and pyridine ring structures of PAA-PVP (Fig. 2). The inter-molecular interaction of PAA and PVP is beneficial to obtain the uniform pore structure.

PAA-PVP electrospun fibers and the PAA-PVP-based carbon fibers were visualized by SEM, as shown in Fig. 3. The electrospun fiber mats were made of random no-woven and an interconnected open structure (Fig. 3a–d). PAA electrospun fibers with warping morphology and average 250 nm in diameter were obtained (Fig. 3a), which due to PAA molecular chain has a large quantity of rigidity structure (Fig. 2). PAA-PVP electrospun fibers have smooth surface (Fig. 3b, c, d), because PVP has better spinnability and more flexibility molecular chain structure compared with PAA. PAA-PVP

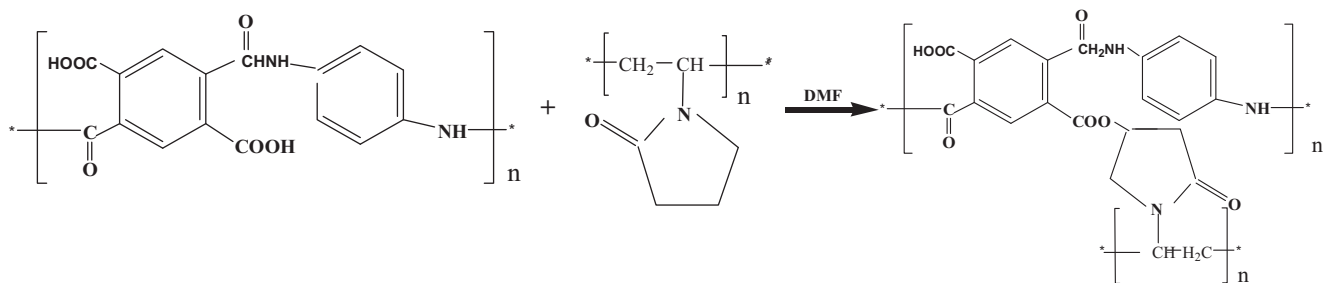


Fig. 2 Schematic illustration of the reaction mechanism of PAA and PVP

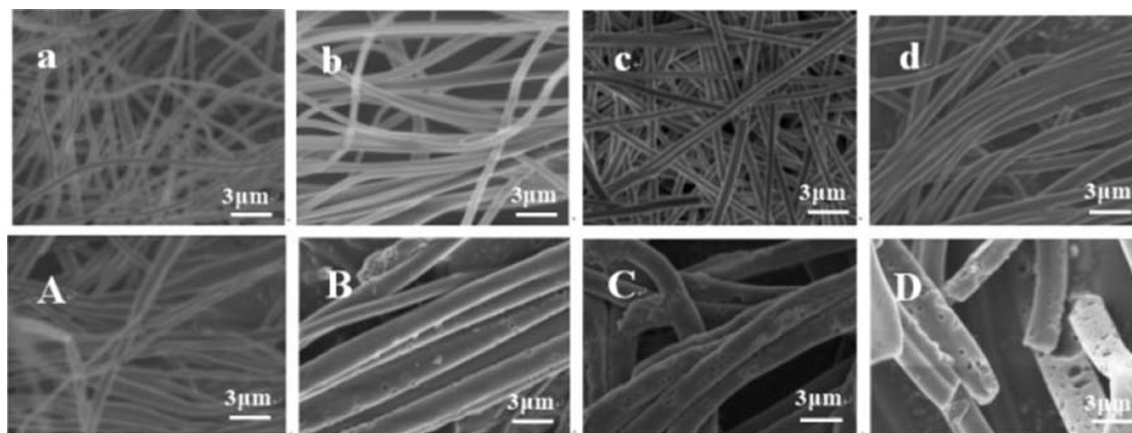


Fig. 3 SEM images of PAA-PVP electrospun fibers and their carbonized fibers. Mass ratio of PAA: PVP (a) and (A) 5:0, (b) and (B) 5:1, (c) and (C) 5:2, (d) and (D) 5:5, respectively

electrospun fibers have 300–500-nm diameter (Fig. 3b, c, d), which due to the linear structure of PVP molecular chain can be easily stretched under electric field force during the electrospinning process, so the smooth surface can be obtained. However, the stretched linear molecular structure of PVP electrospun fiber is also easily shrinkage after withdrawing the electric stress, so the larger average diameter of electrospun fibers was obtained.

Carbon nanofibers derived from PAA electrospun fibers exhibit smooth surface morphology and have no obvious meso/macro pores on the surface, as shown in Fig. 3A. The average diameter of carbon fibers increases to about 300 nm (Fig. 3A), resulting from the influence of thermal decomposition, cyclization, and carbonization of PAA electrospun fibers during the thermal treatment process. Carbon nanofibers obtained from PAA-PVP electrospun fibers can be observed obvious meso/macro pore structure on the surface, as shown in Fig. 3B, C, D. During thermal treatment process, the PAA of PAA-PVP electrospun fibers with high carbon conversion

(Fig. 4a) can produce the carbon matrix structure of carbon nanofibers, the PVP domains of PAA-PVP electrospun fibers with low carbon conversion (Fig. 4b) were removed, so the meso/macro pore structure can be obtained. The esterification reaction between PAA and PVP can ensure the uniform distribution of PAA in PAA-PVP electrospun fibers, so the distribution of meso/macro pores of carbon nanofibers was also uniform (Fig. 3). With the improved content of PVP, the average pore diameter of PAA-PVP-based carbon nanofibers is enlarged (Fig. 3C) and the specific surface area is improved, as shown in Table 1. The average pore size of carbon nanofibers was further enlarged with the further improving content of PVP of PAA-PVP electrospun fiber (Fig. 3D); however, the specific surface area and volume capacity of PAA-PVP-based carbon nanofibers were decreased (Table 1), and the fracture and fragmentation of carbon nanofibers were also be observed from SEM images (Fig. 3D), which damage the integrity of nanofibers. All those are not beneficial to the charge storage and electron/ion transport of carbon nanofibers served as electrode in ILs electrolyte, which can also be demonstrated in the electrochemical measurements of carbon nanofibers (Figs. 6, 7, and 8).

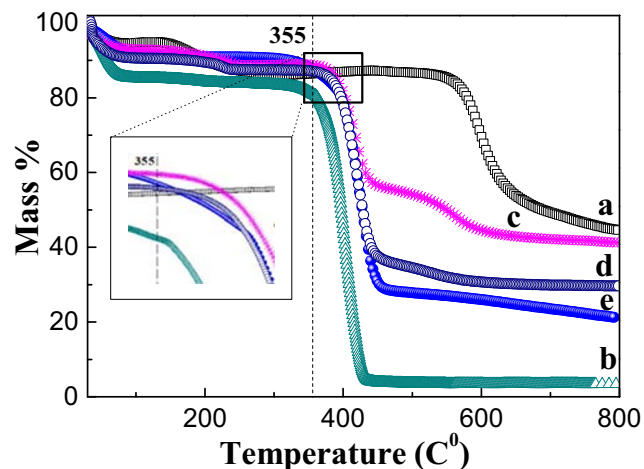


Fig. 4 Thermogravimetric analysis of polymer electrospun fibers. Mass ratio of PAA:PVP (a) 5:0, (b) 0:5, (c) 5:1, (d) 5:2, (e) 5:5

Table 1 Pore structure parameters of carbon nanofibers

Fibers derived from PAA:PVP (mass ratio)	5:0		5:1		5:2		5:5	
Carbonization-activation	Before	After	Before	After	Before	After	Before	After
Average pore diameter (nm)	1.214	1.804	1.151	2.214	1.133	3.101	1.114	4.207
Micro pore capacity (cm ³ g ⁻¹)	0.009	0.037	0.008	0.031	0.008	0.027	0.008	0.026
Meso/macro pore capacity (cm ³ g ⁻¹)	0.004	0.011	0.003	0.072	0.003	0.098	0.003	0.081
Total pore capacity (cm ³ g ⁻¹)	0.013	0.047	0.011	0.099	0.011	0.126	0.011	0.105
Specific surface area (m ² g ⁻¹)	47.3	617.2	37.1	636.2	35.2	743.5	30.5	635.1

45.1 wt% and 3.3 wt%, respectively, which can be calculated from the TG analysis (Fig. 4a, b). The second step of PVP (406 °C and 386 °C; Fig. 4c, d) of PAA-PVP electrospun fibers has a higher decomposition onset temperature than that of PVP electrospun fibers (Fig. 4b). The thermal stability of PVP of PAA-PVP is improved that can be attributed to the esterification reaction between PAA and PVP (Fig. 2), which increases the thermal stability of PVP. Furthermore, the PVP of PAA-PVP electrospun fibers was wrapped by polyimide after the thermal imidization of PAA (280 °C), so the thermal stability of PVP of PAA-PVP electrospun fibers was improved. With the content of PVP of PAA-PVP electrospun fibers further increasing, the influence of polyimide on the thermal stability of PVP was decreased, so the decomposition temperature decreases slightly (380 °C; Fig. 4e). The great majority PVP of PAA-PVP electrospun fibers was removed

after 600 °C (Fig. 4); the carbon conversion of PAA-PVP electrospun fibers can be measured by TG analysis (Fig. 4c, d, e), which is approximately the same to the calculated value according to the carbon conversion of PAA and PVP, respectively, which corresponds to the mass ratio of PAA and PVP in electrospun precursor solution.

The pore structure parameters of carbon nanofibers derived from polymer electrospun fibers are shown in Table 1. BET specific surface area of PAA electrospun fibers is higher slightly than that of PAA-PVP electrospun fibers, because the PAA electrospun fibers have rough surface and small diameter (Fig. 3a). PAA-PVP-based carbon nanofibers show higher BET specific surface area than PAA-based carbon nanofibers, because the thermal decomposition of PVP can produce a high proportion of meso/macro pores (Table 1). Furthermore, volatile gases of small molecular (H₂O, NH₃,

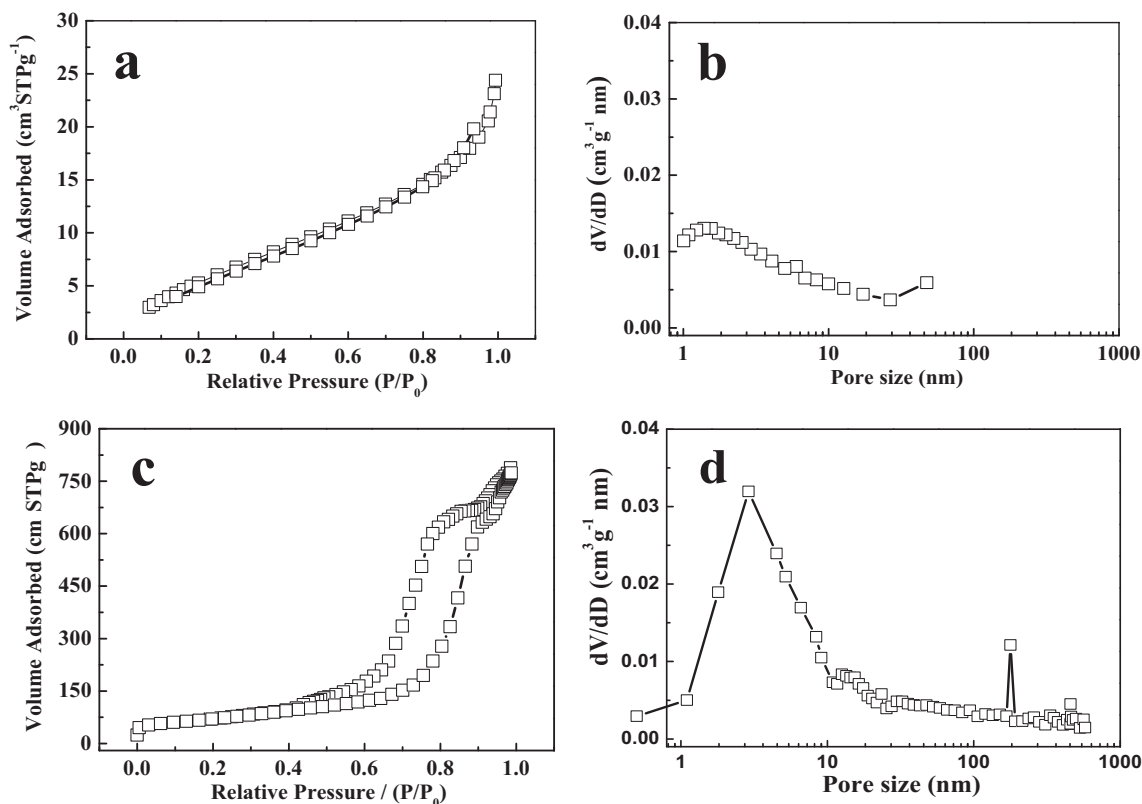


Fig. 5 N₂ adsorption-desorption isotherms and BJH pore size distribution plots **a, b** for PAA-PVP electrospun fibers and **c, d** for its carbonized fibers

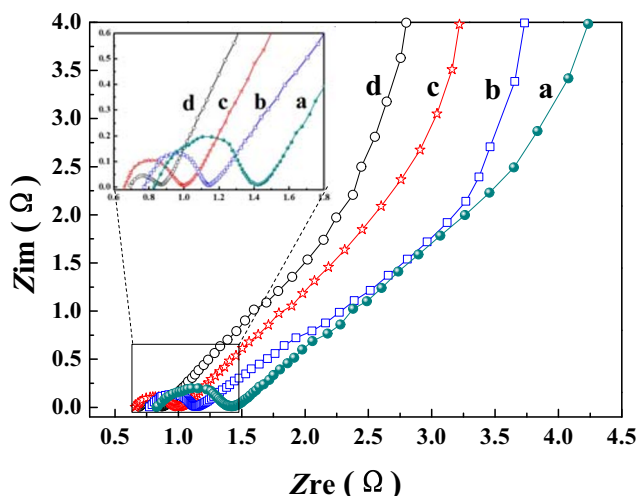


Fig. 6 Alternate current impedance curve of carbon nanofibers supercapacitor. Mass ratio of PAA:PVP (a) 5:0, (b) 5:1, (c) 5:2, (d) 5:5

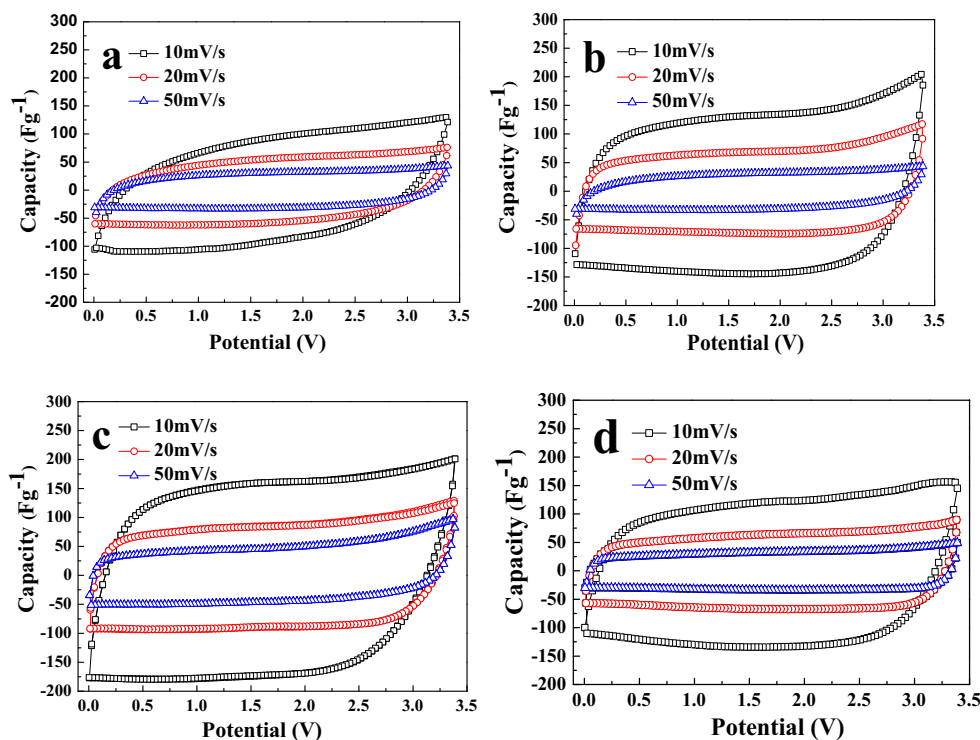
and CO_x etc.) produced from the thermal decomposition of PVP, which can make a penetration through of the meso/macro pore structure by the self-activation process. The interconnected pores are favorable for the improving of ion mobility/diffusibility and utilization efficiency of specific surface areas. However, high PVP content of PAA-PVP electrospun fibers will generate more meso/macro pore structure after thermal treatment (Fig. 3D), so its BET specific surface area decreases (Table 1). Carbon nanofibers derived from PAA-PVP (mass ratio of PAA:PVP = 5:2) show higher BET specific

surface area ($743.5 \text{ m}^2 \text{ g}^{-1}$) and suitable average pore diameter (3.1 nm). The nitrogen adsorption-desorption isotherm and the pore size distribution plots of the PAA-PVP-based carbon nanofibers (mass ratio of PAA:PVP = 5:2) are shown in Fig. 5. PAA-PVP electrospun fibers show a typical III type N_2 adsorption-desorption isotherm of polymer (Fig. 5a) and the low BET specific surface area (Table 1) owing to its low porosity and pore capacity (Fig. 5b). However, the PAA-PVP-based carbon nanofibers show a typical IV type N_2 adsorption-desorption isotherm, which corresponds to the meso/macro pore structure of carbon nanofibers (Fig. 5c). Owing to the suitable average pore size distribution and high pore capacity (Fig. 5d), the PAA-PVP-based carbon nanofibers have high BET specific surface area (Table 1), which is in agreement with the SEM images (Fig. 3c).

Electrochemical feature of carbon nanofibers

The kinetics at the intersurface between the porous carbon nanofibers and the ILs electrolyte were characterized by electrochemical impedance spectroscopy (EIS) analysis, and the Nyquist plots are shown in Fig. 6. The high-frequency region of Nyquist plot represents the charge transport, and the slope of Nyquist plot is related to the formation rate of EDLs at intermediate frequency. The projected length of the Warburg-type plot on the real axis characterizes the ion mobility/diffusibility process from solution into the inter pores of carbon nanofibers. The semicircle describes the impedance

Fig. 7 Cyclic voltammetry curves of porous carbon nanofiber supercapacitor. Mass ratio of PAA:PVP a 5:0, b 5:1, c 5:2, d 5:5



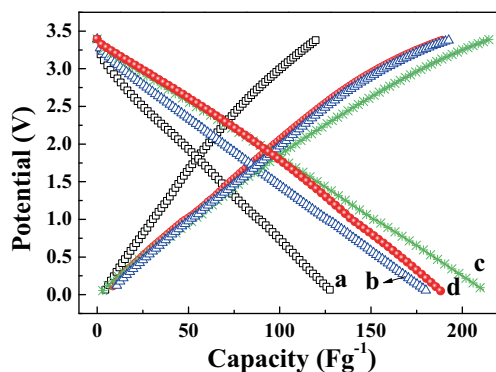


Fig. 8 Constant current charge-discharge curves of carbon nanofiber supercapacitor. Mass ratio of PAA:PVP (a) 5:0, (b) 5:1, (c) 5:2, (d) 5:5

of electrochemical reactions associated with charge transport on the porous carbon fibers. The lower projected slope value and smaller semicircle mean a small charge transfer resistance and the shorter EDLs forming time. The PAA-based carbon nanofibers show smaller projected slope values and big semicircle radius (Fig. 6a), because a large amount of micro pore structure is not beneficial to the ion mobility/diffusibility of ILs with big molecular volume, resulting into a long time for the EDLs forming. PAA-PVP-based carbon nanofibers exhibit larger projected slope and bigger slope (Fig. 6b, c, d), because a large quantities of meso/macro pore structure were produced by using PVP as a sacrificial pore-forming agent, which enables high ion mobility/diffusibility rate of ILs. A high proportion of meso/macro pore structure is beneficial to the mobility/diffusibility, ion buffering reservoirs, and EDLs forming in ILs electrolyte, and those were also further certificated by cyclic voltammogram and linear voltammogram analyses (Figs. 7 and 8). However, the electrical conductivity suffers from a decrease with more macro pore structure (Fig. 6d), because the fracture and fragmentation of carbon nanofibers (Fig. 3D) decrease its conductivity which served as electrode. PAA-based carbon nanofibers featured smaller slope of Nyquist plot at low-frequency area than PAA-PVP-based carbon nanofibers (Fig. 6), indicating a weak frequency response characteristic due to a long EDLs forming time.

The cyclic voltammetry (CV) curves of carbon nanofibers in ILs using various scanning rate in a voltage window of 0.0 V to 3.4 V are shown in Fig. 7. The profiles of CV curves without any oxide reduction peaks exhibit a typical EDLs capacitor. The CV curve of ideal capacitor is rectangle;

however, the CV curve of carbon-based capacitor has some deviation, because the influence of electrolyte ion throughout the inner surface of pores. PAA-based carbon nanofibers had a serious deviation, especially under high current density (Fig. 7a), because the small pore diameter and high aspect ratio of micro pores did not facilitate the ion transport of ILs and form of EDLs, suggesting a weak current response ability to the potential was obtained. PAA-PVP-based carbon nanofibers show higher specific capacity and better power performance than the PAA-based carbon nanofibers (Fig. 7b, c, d). Those electrochemical performances enhanced are due to the high proportion of meso/macro pore structure, which is beneficial to ILs ion throughout the internal porous carbon fibers. [DEMETFSA]BF₄⁻ which served as ILs electrolyte has larger size molecules (diameter parameter of cation = 0.82 nm and anion = 0.23 nm, respectively) and higher viscosity (426 cP), so the meso/macro pore structure provides more active surface area and faster ion mobility/diffusibility for ILs than the micro pore structure. With the pore size increasing, the better response curve of current potential can be obtained (Fig. 7d), because the improved ion mobility/diffusibility and shorten EDLs forming time can be achieved; however, the specific capacity decreases due to the low utilization of pore space (Fig. 7d). The carbon nanofibers derived from PAA-PVP (mass ratio = 5:2) electrospun fibers have suitable pore size, better pore volume, and higher specific surface area (Table 1), which is correspondence in the characters of ILs, so the better comprehensive electrochemical performances than other carbon nanofibers were obtained (Fig. 7c).

The galvanostatic charge-discharge (GCD) tests of carbon nanofiber electrode in ILs were performed for 1000 cycles under 100.0 mA g⁻¹ within 0.0–3.4 V, and the 1000th GCD profiles are presented in Fig. 8. The electrochemical performances were calculated and are summarized in Table 2. The voltage changes linearly over time for a given electrical current, suggesting that only ion adsorption/desorption is involved at the electrode/electrolyte interface without other chemical reactions. PAA-based carbon nanofibers show a bending curve of charge/discharge and a big voltage drops (Fig. 8a and Table 2), because its high proportion of micro pore structure provides low ILs ion mobility/diffusibility, thus needing a long EDLs forming time for ILs. However, the PAA-PVP based carbon nanofibers with high proportion of meso/macro pore structure, which is associated with high

Table 2 Electrochemical performance parameters of carbon nanofiber supercapacitor

Carbon fibers derived from	Specific capacitance (<i>C</i> , F g ⁻¹)	Internal resistance (<i>R</i> , Ω)	Energy density (<i>E</i> , Wh kg ⁻¹)	Power density (<i>P</i> , W kg ⁻¹)	Charge/discharge efficiency (<i>η</i> , %)
PAA	128.1	1.42	10.1	1477	95.0
PAA:PVP = 5:1	180.8	1.15	18.2	1870	95.3
PAA:PVP = 5:2	211.7	1.03	23.1	2021	98.9
PAA:PVP = 5:5	189.5	0.89	19.5	2107	99.2

ion mobility/diffusibility and fast ion adsorption/desorption rate, because the advantage of porous structure as described earlier in the alternative current impedance (Fig. 6) and CV analysis (Fig. 7), so exhibiting smaller voltage drop and higher Coulombic efficiencies (Figs. 8b, 8c, 8d). The carbon nanofibers derived from PAA-PVP (mass ratio = 5:2) exhibit some of the most desirable behavior: high specific capacity (210 F g^{-1}), high power density (2021 W kg^{-1}), charging/discharging efficiency (98.9%), and low internal resistance (1.0Ω), as shown in Table 2.

Conclusions

In summary, porous carbon nanofibers can be obtained via electrospinning of PAA-PVP, thermally induced phase separation, and carbonization processes. PAA with high carbon conversion was converted to the carbon matrix fibers, PVP domains in a PAA matrix served as the pore-forming agent owing to its low carbon conversion, so the porous carbon nanofibers with tunable pore size, specific surface area, and electrical conductivity were prepared by self-assembly, stabilization, and pyrolysis. The porous carbon nanofibers derived from PAA-PVP (mass ratio = 5:2) possess the well-balanced porous structure: high specific surface area ($743.5 \text{ m}^2 \text{ g}^{-1}$), large pore capacity ($0.126 \text{ cm}^3 \text{ g}^{-1}$), and suitable average pore diameter (3.1 nm). A high proportion of meso/macro pore structure of PAA-PVP-based nanofibers as supercapacitor electrode are beneficial for the fast ion transport, high energy storage density, and short EDLs forming. So a comprehensive electrochemical performance can be achieved, such as wide electrochemical stability window (3.4 V), high specific power density (2021 W kg^{-1}), large specific energy density (211.7 F g^{-1}), and low internal resistance (1.0Ω).

Funding information This work received financial supports from the Project of Liaoning Province, China (Nos. 0518XN011, 0519BS014), the National Natural Science Foundation of China (Nos. 21671025, 21471021), and Innovation and Entrepreneurship Training Project of Liaoning Province, China (Nos. 201910167192, 201910167082).

References

- Perumal P, Christopher Selvin P, Selvasekarapandian S (2018) Characterization of biopolymer pectin with lithium chloride and its applications to electrochemical devices. *Ionics* 24:3259–3270
- Hemalatha R, Alagar M, Selvasekarapandian S, Sundaresan B, Moniha V, Boopathi G, Christopher Selvin P (2019) Preparation and characterization of proton-conducting polymer electrolyte based on PVA, amino acid proline, and NH_4Cl and its applications to electrochemical devices. *Ionics* 25:141–154
- Wang K, Zhang WZ, Lou FP, Wei P, Qian ZM, Guo WH (2018) Preparation of electrospun heterostructured hollow SnO_2/CuO nanofibers and their enhanced visible light photocatalytic performance. *J Solid State Electrochem* 22:2413–2423
- Kouchachvili L, Yaici W, Entchev E (2018) Hybrid battery/supercapacitor energy storage system for the electric vehicles. *J Power Sources* 374:237–248
- Rawool CR, Punde NS, Rajpurohit AS, Karna SP, Srivastava AK (2018) High energy density supercapacitive material based on a ternary hybrid nanocomposite of cobalt hexacyanoferrate/carbon nanofibers/polypyrrole. *Electrochim Acta* 268:411–423
- Li B, Zheng JS, Zhang HY, Jin LM, Yang DJ, Lv H, Shen C, Shellikeri A, Zheng YR, Gong RQ, Zheng JP, Zhang GM (2018) Electrode materials, electrolytes, and challenges in nonaqueous lithium-ion capacitors. *Adv Mater* 30:1705670
- Park J, Yoo YE, Mai LQ, Kim W (2019) Rational design of a redox-active nonaqueous electrolyte for a high-energy-density supercapacitor based on carbon nanotubes. *ACS Sustain Chem Eng* 7:7728–7735
- He TS, Jia R, Lang XS, Wu X, Wang YB (2017) Preparation and electrochemical performance of PVdF ultrafine porous fiber separator-cum-electrolyte for supercapacitor. *J Electrochem Soc* 164:E379–E384
- Ye YS, Rick J, Hwang BJ (2013) Ionic liquid polymer electrolytes. *J Mater Chem A* 1:2719–2743
- MacFarlane DR, Forsyth M, Howlett PC, Kar M, Passerini S, Pringle JM, Ohno H, Watanabe M, Yan F, Zheng W, Zhang S, Zhang J (2016) Ionic liquids and their solid-state analogues as materials for energy generation and storage. *Nat Rev Mater* 1:15005
- Béguin F, Presser V, Balducci A, Frackowiak E (2015) Carbons and electrolytes for advanced supercapacitors. *Adv Mater* 26:2219–2251
- Zhang C, Zhang P, Zhang H (2019) Electrospun porous Fe_2O_3 nanotubes as counter electrodes for dye-sensitized solar cells. *Int J Energy Res* 43:5355–5366
- He TS, Meng XL, Nie JP, Tong Y, Cai KD (2016) Thermally reduced graphene oxide electrochemically activated by bis-spiro quaternary alkyl ammonium for capacitors. *ACS Appl Mater Interfaces* 8:13865–13870
- Ding R, Wu H, Thunga M, Bowler N, Kessler MR (2016) Processing and characterization of low-cost electrospun carbon fibers from organosolv lignin/polyacrylonitrile blends. *Carbon* 100:126–136
- Wu C, Zhou TZ, Du Y, Dou SX, Zhang H, Jiang L, Cheng Q (2019) Strong bioinspired HPA-rGO nanocomposite films via interfacial interactions for flexible supercapacitors. *Nano Energy* 58:517–527
- Gupta R, Kumar R, Shama A, Verma N (2015) Novel cu-carbon nanofiber composites for the counter electrodes of dye-sensitized solar cells. *Int J Energy Res* 39:668–680
- Zhao PY, Yu BJ, Sun S, Guo Y, Chang ZZ, Li Q, Wang CY (2017) High-performance anode of sodium ion battery from polyacrylonitrile/humic acid composite electrospun carbon fibers. *Electrochim Acta* 232:348–356
- Chinnappan A, Baskar C, Baskar S, Ratheesh G, Ramakrishna S (2017) An overview of electrospun nanofibers and their application in energy storage, sensors and wearable/flexible electronics. *J Mater Chem C* 5:12657–12673
- Chen LF, Feng Y, Liang HW, Wu ZY, Yu SH (2017) Macroscopic-scale three-dimensional carbon nanofiber architectures for electrochemical energy storage devices. *Adv Energy Mater* 7:1700826
- Frank E, Stuedle LM, Ingildeev D, Spoerl JM, Buchmeiser MR (2014) Carbon fibers: precursor systems, processing, structure, and properties. *Angew Chem Int Ed* 53:5262–5298
- Zhao S, Shi ZQ, Wang CY, Chen MM (2008) Structure and surface elemental state analysis of polyimide resin film after carbonization and graphitization. *J Appl Polym Sci* 108:1852–1856
- Le TH, Yang Y, Yu L, Gao T, Huang Z, Kang F (2016) Polyimide-based porous hollow carbon nanofibers for supercapacitor electrode. *J Appl Polym Sci* 133:43397

23. Le TH, Yang Y, Yu L, Gao T, Huang Z, Kang F (2016) Polyimide-based porous hollow carbon nanofibers for supercapacitor electrode. *J Appl Polym Sci* 133(19):43397
24. Zhou ZP, Liu TY, Khan AU, Liu GL (2019) Block copolymer-based porous carbon fibers. *Sci Adv* 5:6852
25. Zhou Z, Liu T, Khan AU, Liu G (2020) Controlling the physical and electrochemical properties of block copolymer-based porous carbon fibers by pyrolysis temperature. *Mol Syst Des Eng* 5:153–165
26. Tang CB, Tracz A, Kruk M, Zhang R, Smilgies DM, Matyjaszewski K, Kowalewski T (2005) Long-range ordered thin films of block copolymers prepared by zone-casting and their thermal conversion into ordered nanostructured carbon. *J Am Chem Soc* 127:6918–6919
27. Serrano JM, Liu T, Khan AU, Botset B, Stovall BJ, Xu Z, Guo D, Cao K, Hao X, Cheng S (2019) Composition design of block copolymers for porous carbon fibers. *Chem Mater* 31:8898–8907
28. Khan WS, Asmatulu R, Rodriguez V, Ceylan M (2014) Enhancing thermal and ionic conductivities of electrospun PAN and PMMA nanofibers by graphene nanoflake additions for battery-separator applications. *Int J Energy Res* 38:2044–2051
29. Zhang H, Lin CE, Zhou MY, John AE, Zhu BK (2016) High thermal resistance polyimide separators prepared via soluble precursor and non-solvent induced phase separation process for lithium ion batteries. *Electrochim Acta* 187:125–133
30. He TS, Su QY, Yildiz Z, Cai KD, Wang YB (2016) Ultrafine carbon fibers with hollow-porous multilayered structure for supercapacitors. *Electrochim Acta* 222:1120–1127
31. Xi X, Chung DDL (2019) Colossal electric permittivity discovered in polyacrylonitrile (PAN) based carbon fiber, with comparison of PAN-based and pitch-based carbon fibers. *Carbon* 145:734–739
32. He TS, Ren X, Wang YB, Nie JP, Cai KD (2016) Electrochemical performance of reduced graphene oxide in Spiro-(1, 1′)-bipyrrolidinium tetrafluoroborate electrolyte. *Int J Energy Res* 40:1105–1111
33. Sharma S, Dhiman N, Pathak D, Kumar R (2016) Effect of nano-size fumed silica on ionic conductivity of PVdF-HFP-based plasticized nano-composite polymer electrolytes. *Ionics* 22:1865–1872

Publisher's note Springer Nature remains neutral with regard to jurisdictional claims in published maps and institutional affiliations.